Dynamic Response of Coarse Granular Material to Wave Load

Ibsen, Lars Bo

Published in:
Dynamics of Structures 1993-1997

Publication date:
1998

Document Version
Publisher's PDF, also known as Version of record

C.2

Dynamic Response of Coarse Granular Material to Wave Load

Lars Bo Ibsen
Department of Civil Engineering, Aalborg University
DK-9000 Aalborg, Denmark

ABSTRACT: The soil beneath vertical breakwaters is subjected to a combination of forces induced by the waves. The forces acting on the soil can be characterized as (1) static load due to submerged weight of the structure, (2) quasi-static forces induced by cyclic wave loading, and (3) wave impact from breaking waves. The stress conditions in the soil below a foundation exposed to these types of loading are very complex. The key to explain and quantify the soil response beneath a vertical breakwater is to understand the role of the volume changes and to be able to model these correctly. It is shown that the volume changes in soil subjected to static and dynamic loading are controlled by the characteristic line. Experiments have been performed to study the factors that influence the location of the characteristic line in drained and undrained tests for various types of sand and various types of loading. These factors include the relative density, the minor principal stress, the intermediate principal stress, the stress path, and the effects of nonhomogeneous and localized strains. The relation of the characteristic line to other features of static, cyclic and dynamic (rate dependent) soil behavior are explained and illustrated with experimental data.

KEYWORDS: characteristic line, confining pressure, cubical triaxial test, cyclic triaxial test, dilatancy, drained behavior, dynamic behavior, phase transformation line, sand, shear test, stress path testing, triaxial test, undrained behavior

1 INTRODUCTION

The soil beneath vertical breakwaters is subjected to a combination of forces induced by the waves. These forces can be characterized as (1) static load due to the submerged weight of the structure, (2) quasi-static forces induced by cyclic wave loading, and (3) wave impact from breaking waves on the vertical wall. A detailed explanation of the wave induced forces are given De Groot et al. (1996). The stress conditions in the soil below a foundation exposed to these types of loads are very complex, as illustrated in Figure 1.

The behavior of granular materials can normally be accurately characterized by results from drained tests, since the materials can be considered fully drained in many practical problems. However, if the rate of loading is very high, such as that resulting from impact forces from breaking waves on vertical breakwaters, then essentially undrained conditions can exist. In addition, if the dimensions of the breakwater is large and the permeability of the cohesionless soil is relatively low, significant pore-pressure changes may develop as a result of the quasi-static forces induced by cyclic wave loading.

To model and predict this complex soil-structure interaction, a reliable soil model is required, which describe the basic phenomena related to soil behavior during static, cyclic, and dynamic loading. Laboratory testing makes it possible to study soil behavior in detail under controlled and well known conditions. By studying the basic phenomena in triaxial tests under uniform conditions, it has been discovered that identical phenomena characterize the sand behavior when subjected to static and dynamic loading. The key to explain and quantify the soil response beneath a vertical breakwater is to understand the role of the volume changes and to be able to model these correctly.

Volume changes are important for the behavior of soils whether under drained or undrained conditions and whether exposed to static, cyclic, or dynamic loading. Volume changes can be contractive or expansive in nature. Expansive or dilative volume changes are most pronounced for dense sands at low confining pressures and high stress levels approaching failure. The transition from compressive behavior observed at lower stress levels to dilative behavior at high stress levels occurs along a straight line through the origin of the stress space. For

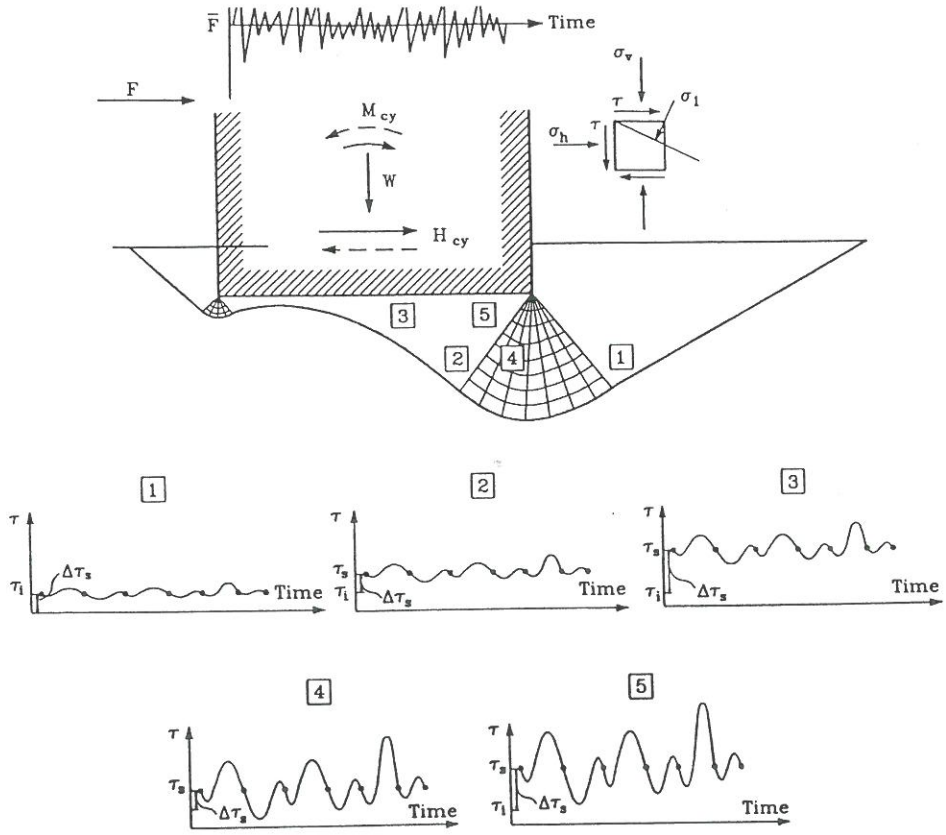

Figure 1. Example of stress conditions for specific elements in the soil below a vertical monolithic structure exposed to static and stochastic non-stationary loads.

drained tests, this line is referred to as the characteristic line.

In elasto-plasticity models the characteristic line, evaluated from $p' = const$ tests, corresponds to the point on the plastic potential surface where the plastic strain increment vector is perpendicular to the p'- axis or the hydrostatic axis (Ibsen and Lade 1998). This state is therefore comparable to the similar point on the yield surface at which the normal is perpendicular to the hydrostatic axis. This indicates the point at which sand may become unstable, as explained in detail elsewhere (Lade *1995).* Thus, the characteristic line plays a similarly important role for the plastic potential surface as the instability line plays for the yield surface. Both lines are shown on the diagram in Figure 2. The behavior of soils is greatly influenced by and may be explained in view of the relative locations of these two lines. For sands the two lines are distinctly separate, while for normally consolidated, insensitive clays the two lines coincide, and they also coincide with the critical state or ultimate state line.

Experiments have been performed to study the factors that influence the location of the characteristic line in drained and undrained tests for various types of sand and various types of loading. These factors include the relative density, the minor principal stress, the intermediate principal stress, the stress path, and the effects of nonhomogeneous and localized strains. The relation of the characteristic line to other features of soil behavior during static, cyclic, and dynamic loading are explained and illustrated with experimental data.

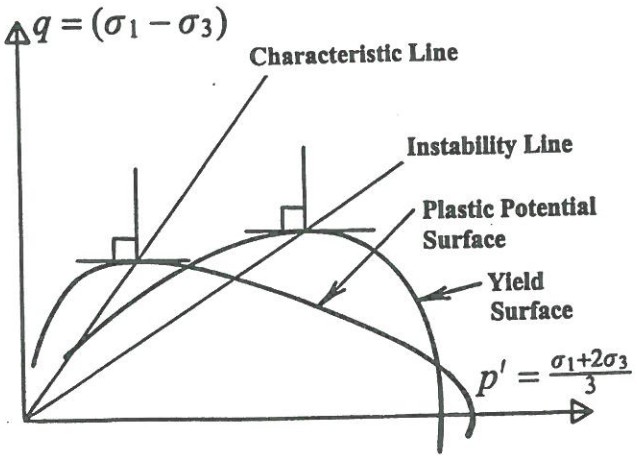

Figure 2. Comparison of characteristic and instability lines.

2. TEST PROGRAM

The tests performed in connection which this project were conventional static CD-tests, $CU_{u=0}$-tests, and cyclic and dynamic CU-tests. The cyclic and dynamic CU-tests were performed as undrained tests with pore pressure measurements. The $CU_{u=0}$-tests were carried out by measuring the volume change and controlling the cell pressure in such a way that $\delta\varepsilon_v = 0$ throughout the test. In this way the undrained condition is ensured and the effective stress path is followed throughout the test.

In conventional triaxial tests the loads, deformations, volume changes or pore pressure are measured outside the specimen, and homogeneous conditions must exist inside the specimen to calculate the correct values of stresses, strains and void ratios throughout the test. Although it has been advocated since 1965 that triaxial tests should be performed on specimens with lubricated cap and base (Rowe and Barden 1964), and height equal to diameter (Bishop and Green 1965 Jacobsen 1967, Lade 1982), it is often considered that sufficiently uniform conditions are achieved by using tall specimens with heights greater than or equal to two diameters.

Ibsen (1994) found that specimens with double height developed nonuniformities in strains resulting in measurements of incorrect stress-strain relations of the material. During undrained conditions the nonuniform development in volumetric strains results in inner draining and consequent generation of erroneous pore pressures. Basic phenomena in soils under drained or undrained conditions, must be studied in test performed on specimens with height equal to diameter and with smooth end plates. This is the best way to ensure that the real stress-strain behavior is determined, while properties of soils obtained from tall specimens may reflect test errors.

To ensure homogeneous stress and strain conditions, the tests presented here were performed on cylindrical specimens with a height and diameter equal to 70 mm, and bounded by lubricated caps and bases. The tests were performed in a newly developed version of the Danish Triaxial Apparatus in which control of stress path, measurement, and data analysis is automated (Ibsen 1994).

The static triaxial specimen was loaded by a mechanically controlled piston, while the dynamic test is loaded by a hydraulic piston. The static tests were performed with constant deformation rate of 4 % per hour, and the dynamic tests were conducted with constant deformation rate varying from 40 to 100,000 % per hour. The measuring systems in the two apparatuses were identical and consisted of electronic load, pressure, and deformation transducers. The working principles of triaxial cell is similar to those described by Jacobsen (1970).

The study described in this paper is based on tests performed on two uniform sands: Aalborg University sand No. 1 and Lund sand No 0. The index properties for these sands are shown in the Table 1.

Table 1. Index Properties.

Property	Aalborg University sand No 1	Lund sand No 0
$d_{50\ mm}$	0.14	0.4
C_U	1.78	1.7
d_s	2.65	2.65
e_{max}	0.86	0.82
e_{min}	0.55	0.55

The test specimens were prepared by a pluvial deposition and carefully saturated in total vacuum (approx. -98 kPa). This causes all specimens to be pre-consolidated to approximated 100 kPa during the preparation process. This technique ensures homogeneous and totally saturated specimens. The triaxial test series was performed on isotropically consolidated specimens with relative densities as shown in Table 2. The test results are reported by Ibsen (1990), Ibsen and Bødker (1994), Jacobsen and Simonsen (1994), and Ibsen and Jacobsen (1996).

Table 2. Relative densities for sand specimens in static triaxial tests.

	Relative densities
Aalborg University sand No. 1	0.10, 0.51, 0.80, 1.00
Lund sand No. 0	0.48, 0.78, 0.93, 1.00

The parameters that describe the state of the soil under axisymmetrical stress conditions, are calculated from the measurements taken during the tests. These parameters are:

the cell pressure σ_3'
the mean normal stress $p' = \frac{1}{3}(\sigma_1' + 2\sigma_3')$
the deviator stress $q' = \sigma_1' - \sigma_3'$
the volumetric strain ε_v
the deviator strain $\varepsilon_q = \frac{2}{3}(\varepsilon_1 - \varepsilon_3)$

where σ_1' is the vertical and σ_3' the horizontal principal stresses. The stresses are effective and ε_1 and ε_3 are the principal strains.

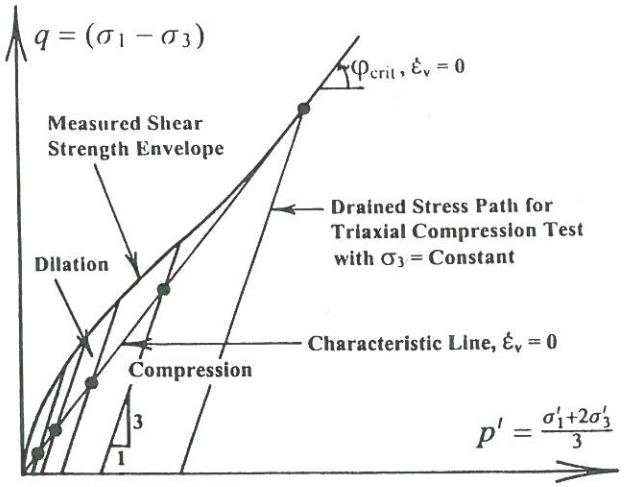

Figure 3. Variation of drained shear strength envelope for sand with constant confining pressure (Lade and Ibsen 1997).

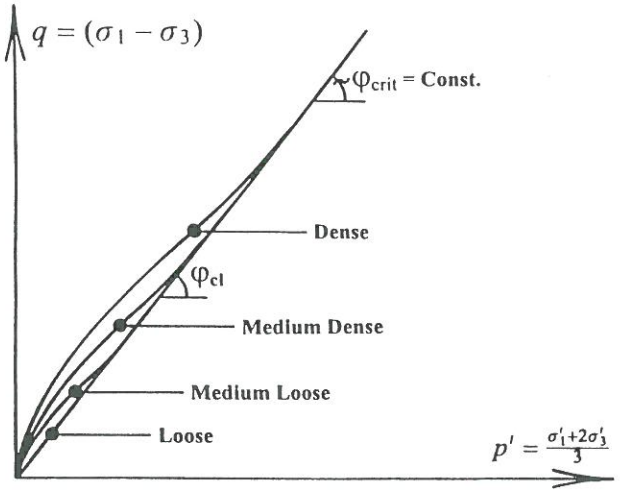

Figure 4. Variation of drained shear strength envelope for sand with relative density. (Lade and Ibsen 1997).

3 DRAINED SHEAR STRENGTH OF SAND

The typical variation of drained shear strength of sand with mean effective stress is illustrated schematically in Figure 3. For a sand with a given initial density, the peak friction angle, φ'_{peak}, consists of two components. One from the basic friction between sand particles modified for contributions from rearrangement of particles at constant volume. The resulting friction angle is referred to as the critical friction angle, φ_{cr}. The second component derives from the dilation of the sand during shear, ψ_{peak}. This relation can be expressed as:

$$\varphi'_{peak} = \varphi'_{cr} + \psi_{peak} \qquad (1)$$

The dilation is suppressed at higher pressures due to crushing, and the resulting strength component therefore reduces to zero at very high pressures.

Thus, a curved failure surface is observed. Experiments on sands have shown that both the contribution from dilation and the range of confining pressures in which dilation occurs reduce with decreasing relative density, as shown schematically in Figure 4.

4. THE CHARACTERISTIC STATE

Figure 5 shows the results of four CD-tests. The tests are performed with different cell pressures, σ'_3, which are held constant throughout each test. Failure is seen to be well defined as the state in which the deviator stress q' is a maximum, as shown in Figure 5b. In this diagram the stress-strain curves are normalized on σ'_3. This causes the curve with the smallest confining pressure to be located at the top. Laboratory tests on several sands have shown that a characteristic threshold exists in granular materials which is defined as the stress state where the volume

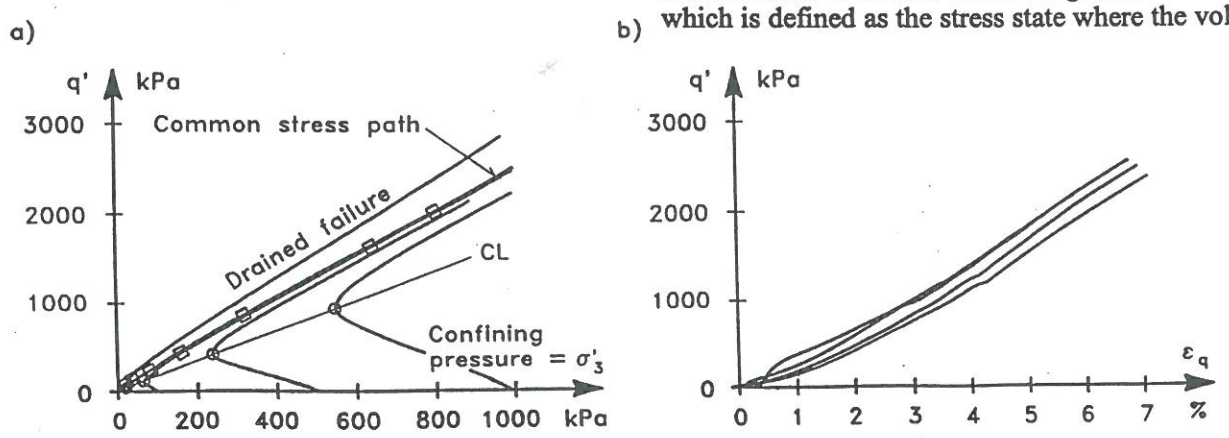

Figure 5. Diagram illustrating the development of stress-strain behavior in CD-tests on dense sand performed with different confining pressures on specimens with equal height and diameter.

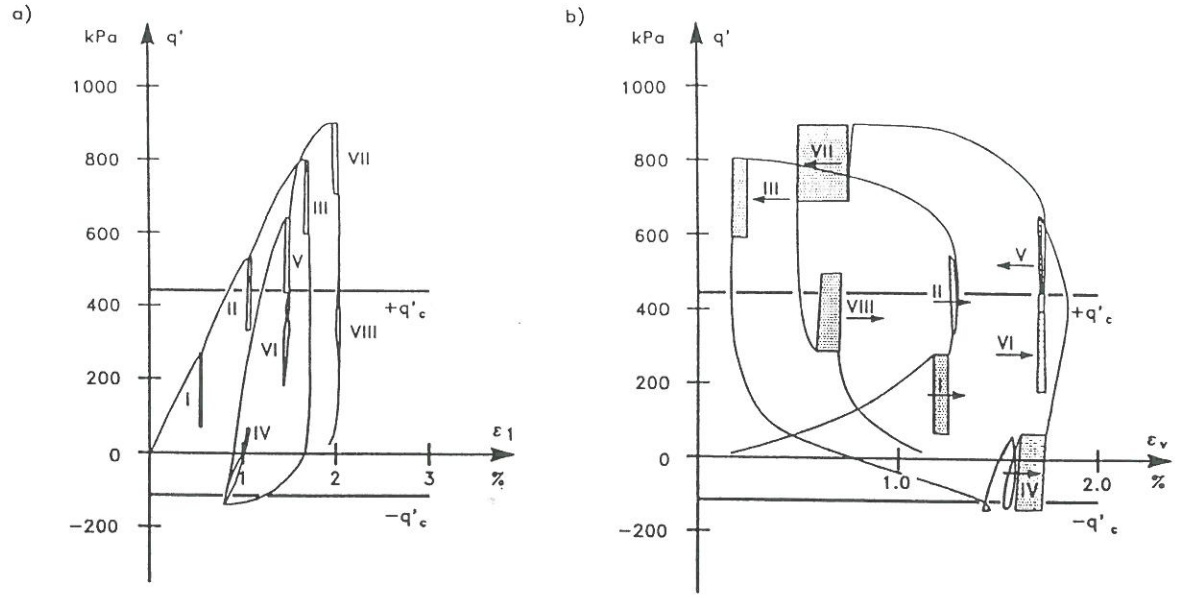

Figure 6. Cyclic loading under constant confinement condition σ'_3 = 200 kPa performed on Fountainbleau sand I_D = 0.64 (Luong 1982).

change goes from contraction to dilation. On the $\varepsilon_1 - \varepsilon_v$ curve, Figure 5c, the characteristic threshold is marked by open circles at the point where the specimen has minimum volume. The stress state characterized by (p_{cl}, q_{cl}) where $\delta\varepsilon_v/\delta\varepsilon_1 = 0$ is defined and described as the *Characteristic State,* (Luong 1982). Characteristic states occur at the transition from contraction to dilation, and these states are located on a line, the *Characteristic Line cl*, through the stress origin. The slope of the characteristic line may be described by an angle, φ_{cl}. The characteristic state and the critical state are very similar, as discussed by (Luong 1982). For loose sand and sand at high confining pressure, $\delta\varepsilon_v/\delta\varepsilon_1 = 0$ is reached at the critical state. The critical state is therefore the same as the characteristic state, and it occurs at failure for sand that compresses during shear. For dense sand or sand at low confining pressure, the characteristic state is reached at small strain magnitudes, as indicated by open circles in Figure 5b, while the critical state is reached at large strains.

The characteristic line divides the stress space into two subspaces in which the stress combinations lead to different deformation mechanisms.

Below the characteristic line the stress combinations lead to contraction, i.e. $\delta\varepsilon_v > 0$.
Above the line the stress combinations lead to dilation, i.e. $\delta\varepsilon_v < 0$.

Below the characteristic line the resistance to deformation is governed by sliding friction due to microscopic interlocking depending upon surface roughness of the particles or interlocking friction between particles. According to (Luong 1982), the resistance is due to pure friction and the characteristic state describes an intrinsic parameter which defines a characteristic angel φ_{cl} for a given sand. In the subspace situated between the failure envelope and the characteristic line the resistance to deformation is governed by disrupture of the interlocking and volumetric dilation.

In Figure 6 cycling sequences are carried out at different deviator stress levels under drained conditions and at constant confinement, $\sigma'_3 = 200$ kPa. Each cycling sequence consists of 20 cycles with a amplitude of 100 kPa. The diagram shows very clearly that the contracting behavior of the soil is obtained when the mean deviator stress level is lower than the characteristic level. The dilation behavior of the soil during load cycling is evident when the mean deviator stress level becomes higher than the characteristic threshold, q'_{cl}.

Loung (1982) has observed that the contraction decreases when the characteristic threshold is approached and dilation increases when deviator stresses increase further. The contraction effect is more pronounced for extension loading having $q' < 0$.

4.1 Effects of Relative Density and Minor Principal Stress

The characteristic angles for drained triaxial compression tests on Aalborg University sand No.1 and Lund sand No.0 at four relative densities, I_D, are shown in Figures 7 and 8. The experiments in these two tests series, in which the relative density varied from 0.01 to 1.0, show that the characteristic angle φ_{cl} is constant and independent of (1) relative density for a given sand, and (2) confining pressure or minor

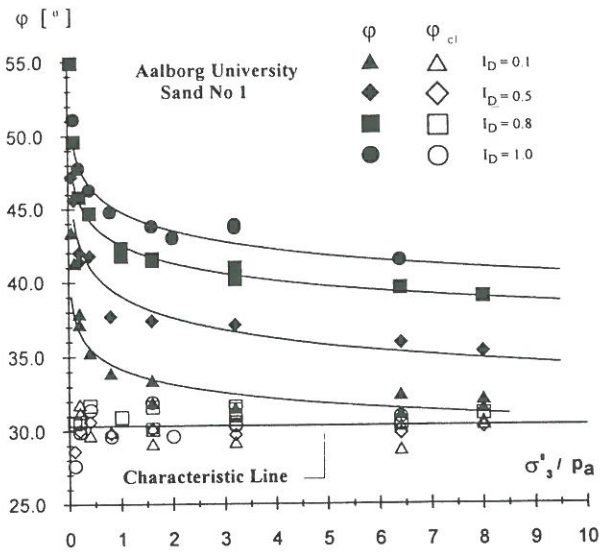

Figure 7. Characteristic angles obtained from triaxial compression tests on Aalborg University Sand No. 1.

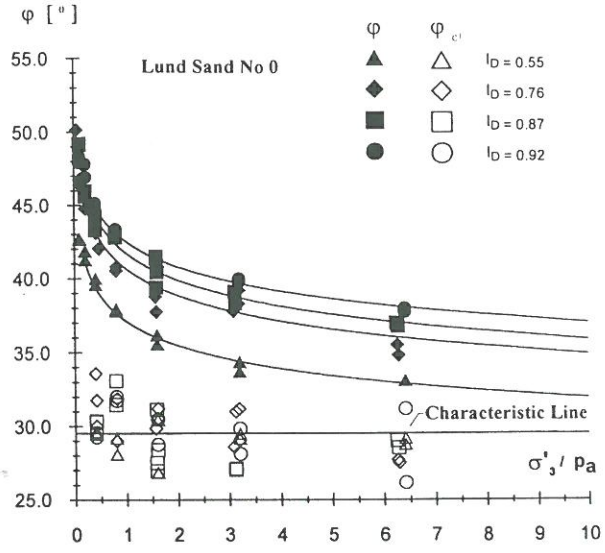

Figure 8. Characteristic angles obtained from triaxial compression tests on Lund No. 0.

principal stress. These observations were also made by Loung (1982).

As discussed in connection with Figure 17, the determination of the stress state at which $\delta\varepsilon_v = 0$ is not necessarily very accurate, because the volume change curve is relatively flat near the characteristic state, while the stress state varies considerably. Therefore, the determination of the characteristic stress points shows some scatter. The characteristic angle for Aalborg University sand No. 1 is found to be $\varphi_{cl} = 30.3^0$ and for Lund sand No.0 it is $\varphi_{cl} = 29.5^0$ These angles are determined according the definition used by Luong (1982).

4.2 Effects of Specimen H/D-Ratio

The characteristic stress states corresponding to $\delta\varepsilon_v = 0$ for triaxial compression tests on Santa Monica Beach sand at four relative densities (Lade and Prabucki 1995) are shown in Figure 9. These experiments were performed on specimens with height-to-diameter ratio $H/D = 2.65$ and with lubricated ends. They also show that the characteristic angle, φ_{cl}, is independent of relative density for a given sand, but due to the development of nonuniformities in strains, the angle is found to vary slightly with the minor principal stress.

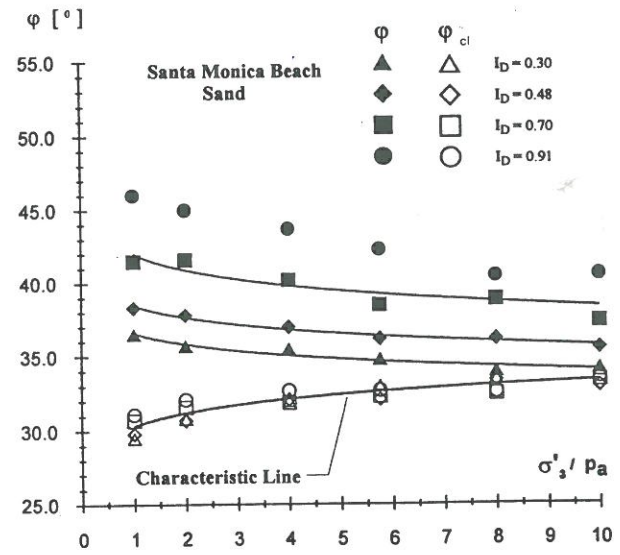

Figure. 9 Characteristic states obtained from triaxial compression tests on Santa Monica Beach Sand.

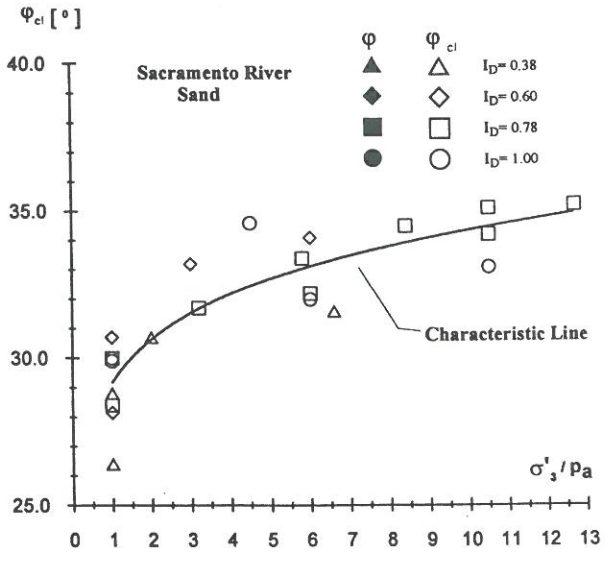

Figure. 10 Characteristic states obtained from triaxial compression tests on Sacramento River Sand.

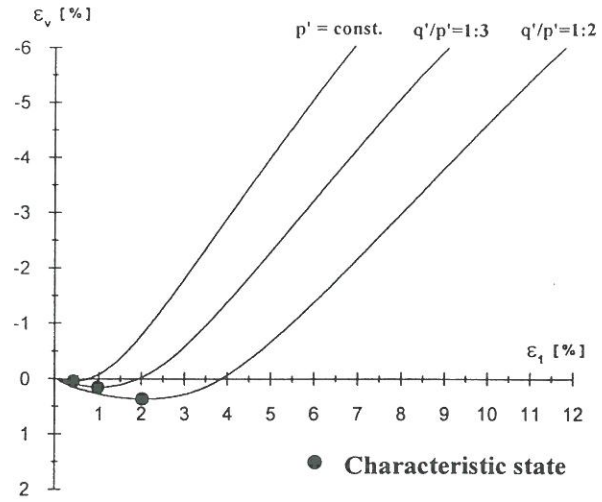

Figure 11. Volumetric curves obtained by stress path tests on Aalborg University sand No. 1, I_D = 1.00. Isotropic consolidated to $\sigma'_3 = 20$ kPa before shearing.

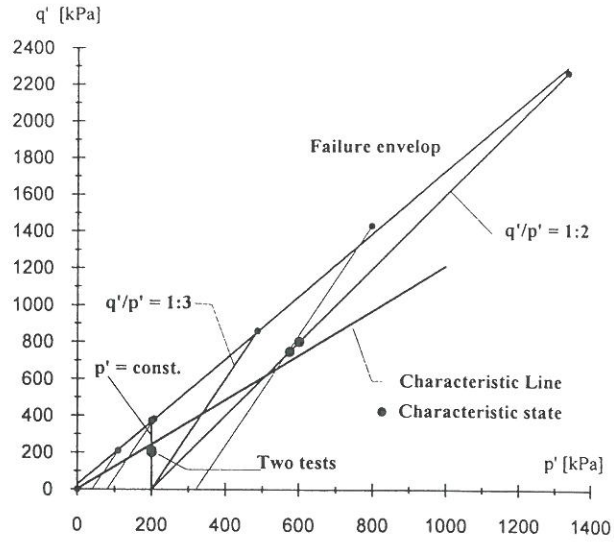

Figure 12. Stress path tests obtained from triaxial compression tests on Aalborg University sand No. 1, $I_D = 1.00$.

The characteristic angles for drained triaxial compression tests on Sacramento River sand (Lee 1965, Lee and Seed 1967) were also determined for four different relative densities, and they are shown in Figure 10. These tests were performed on specimens with $D = 3.56$ cm and $H/D = 2.43$, and without lubricated ends. The data for Sacramento River sand shows more scatter than the other test series. Still, the tests indicate that the characteristic angle is independent of relative density. Due to the more pronounced nonuniformities in stress and strains caused by rough end plates, the characteristic angles vary more with confining pressure than the data for Santa Monica Beach sand. It is therefore important to realize that the nonuniform deformations, which develop at very small strains, influence the measured characteristic angles and therefore the conclusions regarding the effect of the minor principal stress.

4.3 Effects of stress path testing

The characteristic stress state discussed above is that observed in conventional triaxial compression tests in which the stress path corresponds to constant confining pressure and $\delta q'/\delta p' = 1/3$. The volumetric strain curves from three triaxial test on Aalborg University sand No. 1 conducted with different stress path are shown in Figure 11. The tests were all performed on specimens with $I_D = 1.00$ and consolidated to a mean normal stress of $\sigma'_3 = 200$ kPa before shearing. The corresponding stress paths $\delta p' = const$, $\delta q'/\delta p' = 1/3$ and $\delta q'/\delta p' = 1/2$ are shown in Figure 12.

Contraction and dilation can be caused by application of shear stresses as well as by changes in the mean normal stress. In the constant p'-test the increment $\delta p'$ is zero and the elastic volumetric strain increment is therefore also zero. In this test the volumetric strains are caused entirely by shear stresses. The test shows shear-induced contraction in the beginning, and it is possible to define a characteristic state, as shown in Figure 11. As expected, the contraction becomes more pronounced as the stress ratio $\delta q'/\delta p'$ increases, and there are distinct differences between the characteristic states obtained from different stress paths, as shown in Figure 11.

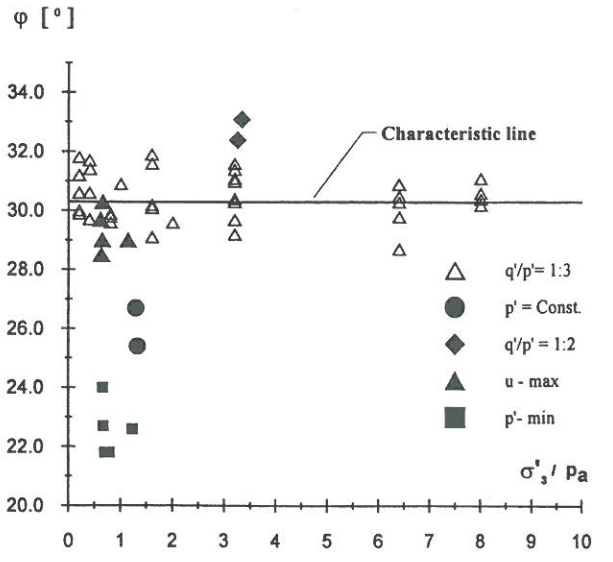

Figure 13. Angles of the characteristic, phase transformation and u_{max} stress states evaluated from drained and undrained triaxial tests on Aalborg University sand No. 1.

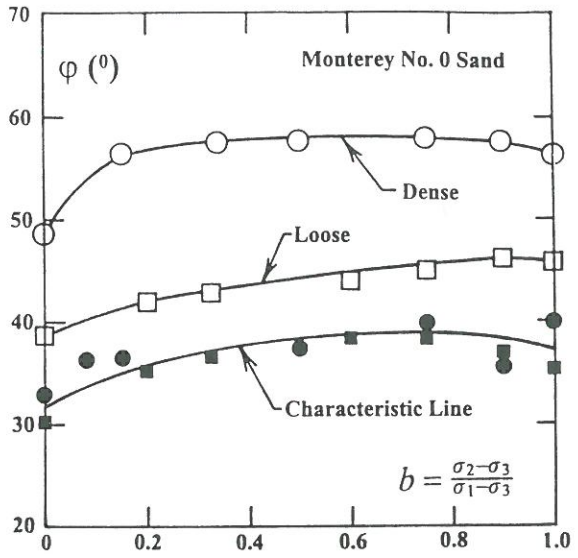

Figure 14. Characteristic angles obtained from cubical triaxial tests on Monterey No. 0 sand.

The characteristic stress states from the three volumetric strain curves are plotted in Figure 12. The characteristic line determined from the results in Figure 7 and two experiments for each of the conditions, $p' = const$ and $\delta q'/\delta p' = 1/2$, are also plotted in this diagram. The characteristic stress states from the $p' = const$ tests are located below and the stress states form the $\delta q'/\delta p' = 1/2$ are located above the characteristic line. The characteristic angle φ_{cl} from these four tests are also plotted in Figure 13. It is seen that φ_{cl} from the $p' = const$ tests is 26°, and it is 33° in the tests with the stress path $\delta q'/\delta p' = 1/2$. The characteristic angles are outside the general scatter of the $\delta q'/\delta p' = 1/3$ tests, and it appears from these experiments that the characteristic stress state and therefore the characteristic angle is a function of the stress path.

4.4 Effects of intermediate principal stress

The characteristic angles have also been obtained from drained cubical triaxial compression tests on dense and loose Monterey No.0 sand (Lade and Duncan 1973) and shown in Figure 14. The characteristic angles are affected by the intermediate principal stress in a similar fashion as the measured friction angles. Each b-value represents a different stress path in the stress space, and there does not seem to be any pronounced effect of relative density on the characteristic angles. It is observed that for a given stress path, the characteristic stress states are independent of relative density.

5 COMPARISON OF PHASE TRANSFORMATION AND CHARACTERISTIC STRESS STATES

The phase transformation stress state plays a similar role for undrained tests as the characteristic stress state plays for drained tests. Figure 15 shows a schematic illustration of the stress state at which phase transformation occurs along an effective stress path from an undrained test. It is the point at which "the stress path turns its direction in p'- q' space" (Ishihara et al. 1975), i.e. the point where the effective stress path has a "knee" and the effective mean normal stress reaches a minimum value p'_{min}. Ishihara et al. (1975) observed that for cyclic undrained triaxial tests "it is necessary for a sample to go at least once through this critical value in order to be taken to a completely liquefied state." In this sense, "the critical stress ratio may be considered as a threshold at which the behavior of sand as a solid is lost and transformed into that of a liquefied state."

Whereas the "knee" described above does not clearly define the location of the phase transformation point, the most consistent definition is one that is independent of the stress path. The phase transformation state is therefore best defined as the point at which the effective stress path has a vertical tangent. This also corresponds to the transition from compressive to dilative behavior. At this point of the undrained test, the increment $\delta p'$ becomes zero, and the elastic volumetric strain increment, $\delta\varepsilon_v^e$, is therefore also zero. Consequently, the plastic volumetric strain increment, $\delta\varepsilon_v^p$, is also zero. This definition theoretically makes the characteristic and phase transformation states identical.

Inspection of the data in Figure 13 shows that the characteristic angles obtained from $p' = const$ tests are slightly higher than the angles defining the phase transformation states. It was expected that the characteristic angle from $p' = const$ tests and the

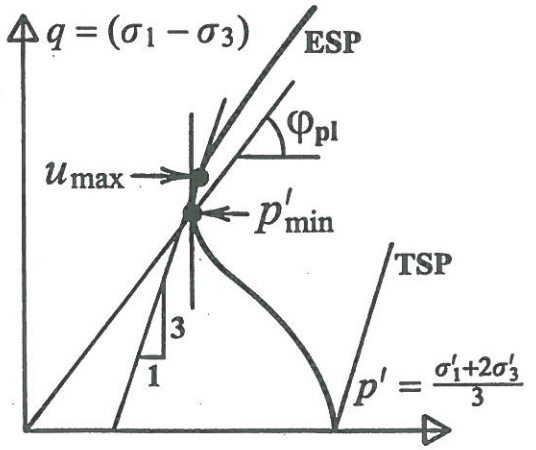

Figure 15 Schematic diagram of phase transformation state in undrained triaxial compression test on sand.

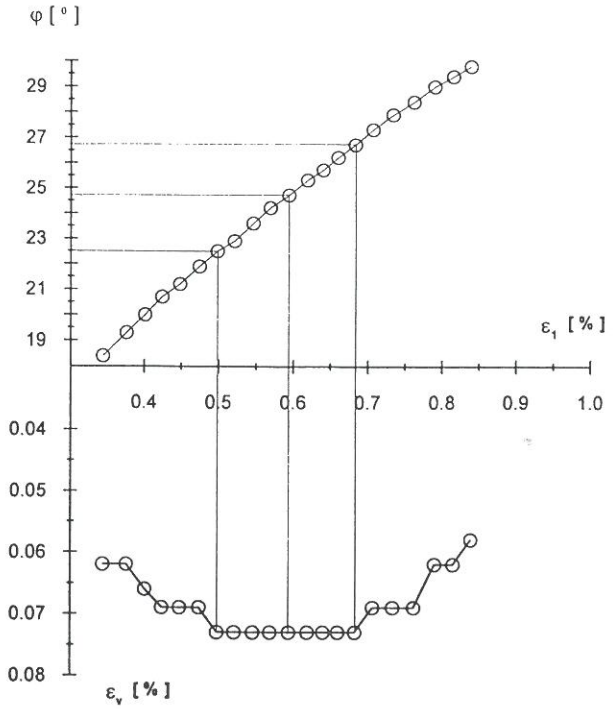

Figure 16. The measured points used to define the characteristic stress state in a p' = constant triaxial test run on Aalborg University sand No. 1 with $I_D = 1.00$.

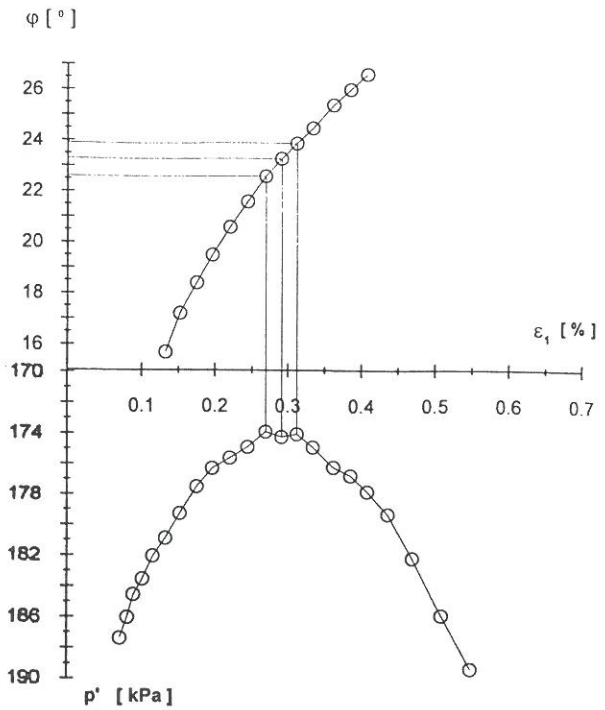

Figure 17. The measured points used to define the phase transformation stress state in a CU triaxial test performed on Aalborg University sand No. 1 with $I_D = 1.00$.

angle of the phase transformation states would be the same, because both stress states are characterized by having $\delta\varepsilon_v^e = 0$. However, the conditions defining the two stress states are not exactly identical. In the undrained test, the total volumetric strain is zero and the elastic and plastic volumetric strains therefore have to compensate for each other, i.e. $\varepsilon_v^e = -\varepsilon_v^p$, while $\varepsilon_v^e = 0$ and $\varepsilon_v^p \neq 0$ in the drained test.

In Figures 16 and 17 the points used to define the characteristic and phase transformation stress states are shown for tests performed on Aalborg University sand No. 1 with $I_D = 1.00$. Figure 16 shows that the transition zone in which $\delta\varepsilon_v = 0$ starts at $\varphi = 22.5°$ and ends at $\varphi = 26.7°$. Previously, and according to Luong (1982), the characteristic stress state has been defined as the mean value in this transition zone producing $\varphi_{cl} = 24.6°$. In comparison, the transition zone for the phase transformation state in the corresponding undrained test is much narrower.

Redefining the characteristic and phase transformation states as the states where $\delta\varepsilon_v$ and $\delta p'$ becomes zero for the first time, produces identical states, if simultaneously, the characteristic state is obtained from a $p' = const$ test, as shown in Figures 16 and 17.

This new definition is used in evaluating the angles shown in Figure 18. The test data are identical with those shown in Figures 7 and 13 for I_D = 1.00. It is seen that the by using this definition, all the characteristic angles, evaluated from CD-tests performed with $p' = const$, become identical with the angles of the phase transformation states. The characteristic angle still shows the same stress path dependency as before, while that evaluated from

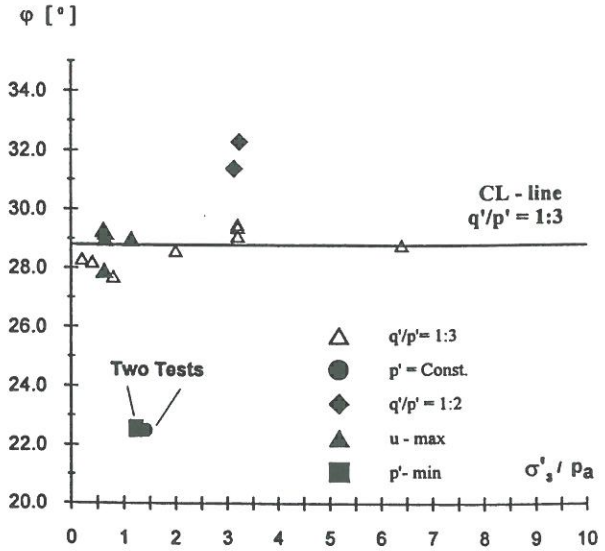

Figure 18. Angles of characteristic and phase transformation states defined as the stress state where $\delta\varepsilon_v$ respectively $\delta p'$ becomes zero. The tests are run on Aalborg University Sand No 1.

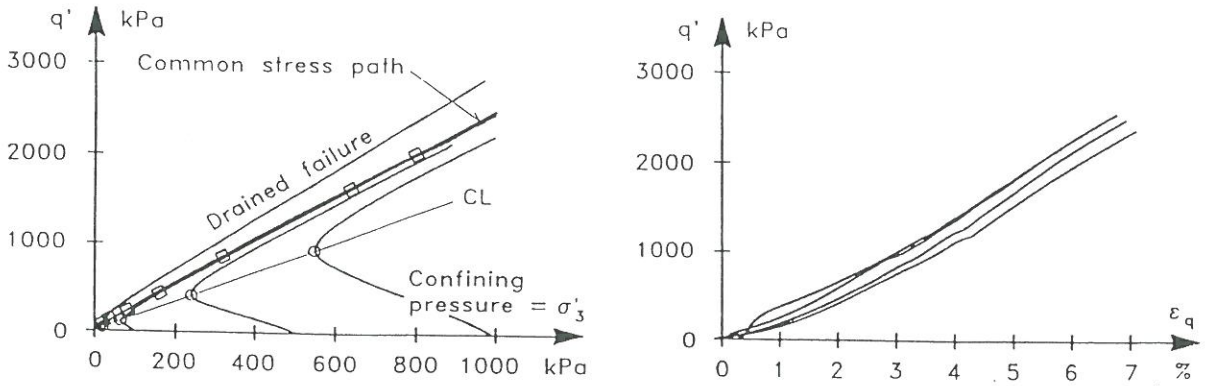

Figure 19. Results of four $CU_{u=0}$ - tests performed on Lund sand No. 0 with I_D = 0.78. The tests were performed on specimens with equal height and diameter.

conventional triaxial tests is reduced from $\varphi_{cl} = 30.3°$ to $\varphi_{cl} = 28.8°$.

6 THE CHARACTERISTIC STATE FOR UNDRAINED CONDITIONS

Along the effective stress path in a undrained test the elastic and plastic volumetric strains have to compensate for each other, i.e. $\varepsilon_v^e = -\varepsilon_v^p$. It has been shown that changes in the effective mean normal stress p' affects both the elastic volumetric strain and the stress state where the soil goes from compression to dilation. In a conventional undrained triaxial compression test, in which the total stress path corresponds to $\delta q'/\delta p' = 1/3$, the phase transformation state does not correspond to the transition from contractive to dilative behavior, i.e. the point where the maximum pore water pressure u_{max} occurs.

The characteristic stress state, as defined by Luong (1982), together with the total stress path, controls the point where the maximum pore water pressure u_{max} occurs in an undrained test. During undrained shear, the pore pressure increases at first in order to prevent the sand from contraction, i.e. $\delta u > 0$. When the deviator stress approaches the characteristic state $\delta u \to 0$. The results of four undrained triaxial tests, shown in Figure 19, indicate that the stress states where $\delta u = 0$ are located on the characteristic line. If q increases further, the effective stress path is located in the subspace which is characterized by dilation. In order to prevent dilation, the pore pressure generation becomes negative, i.e. $\delta u < 0$, as shown in Figure 19a. If the effective stress path in Figure 19a is plotted in a $p' - q$ diagram, the stress state corresponding to maximum pore water pressure u_{max} will occur slightly later than the phase transformation stress state, as indicated in Figure 15.

Stress states corresponding to u_{max} from five undrained tests performed on Aalborg University sand No. 1 with I_D = 1.00, 0.80 and 0.51 are shown in Figure 18. It is seen that u_{max} corresponds to the characteristic stress states for the tests conducted with the stress ratio $\delta q'/\delta p' = 1/3$. It is also recognized that the stress state where u_{max} occurs is quite different from the phase transformation stress state corresponding to p'_{min}.

7 UNDRAINED SHEAR STRENGTH OF SAND

Figure 19a shows that the effective stress path approaches a common stress path asymptotically, defined by the stress state marked with open squares. This common stress path is identical with the stress path defined by the stress states where the total volumetric strain $\Sigma\delta\varepsilon_v = 0$, marked by open squares in Figure 5.

This common stress path is normally considered to be the undrained failure envelope. In Figure 19b it is shown that the common stress path does not represent any failure state in the sand, and tests covering a σ'_3 interval from 5 kPa to 2000 kPa do not reveal any maximum on the stress-strain curves. This conclusion is not in agreement with the state of the art. The state of the art is build on undrained tests performed on specimens with double height and it therefore reflects the test errors and not the real properties of the soil, as explained above and also by Ibsen (1994).

7.1 Failure restricted by undrained conditions

Failure under undrained conditions develops when the pore water fails to prevent dilation. From this state $\delta\varepsilon_v$ is no longer equal to zero and the soil starts to dilate. In this way the failure is controlled by the same mechanism as failure under drained conditions. The stress path followed can be explained in view of the relative locations of the characteristic stress state and the drained failure surface.

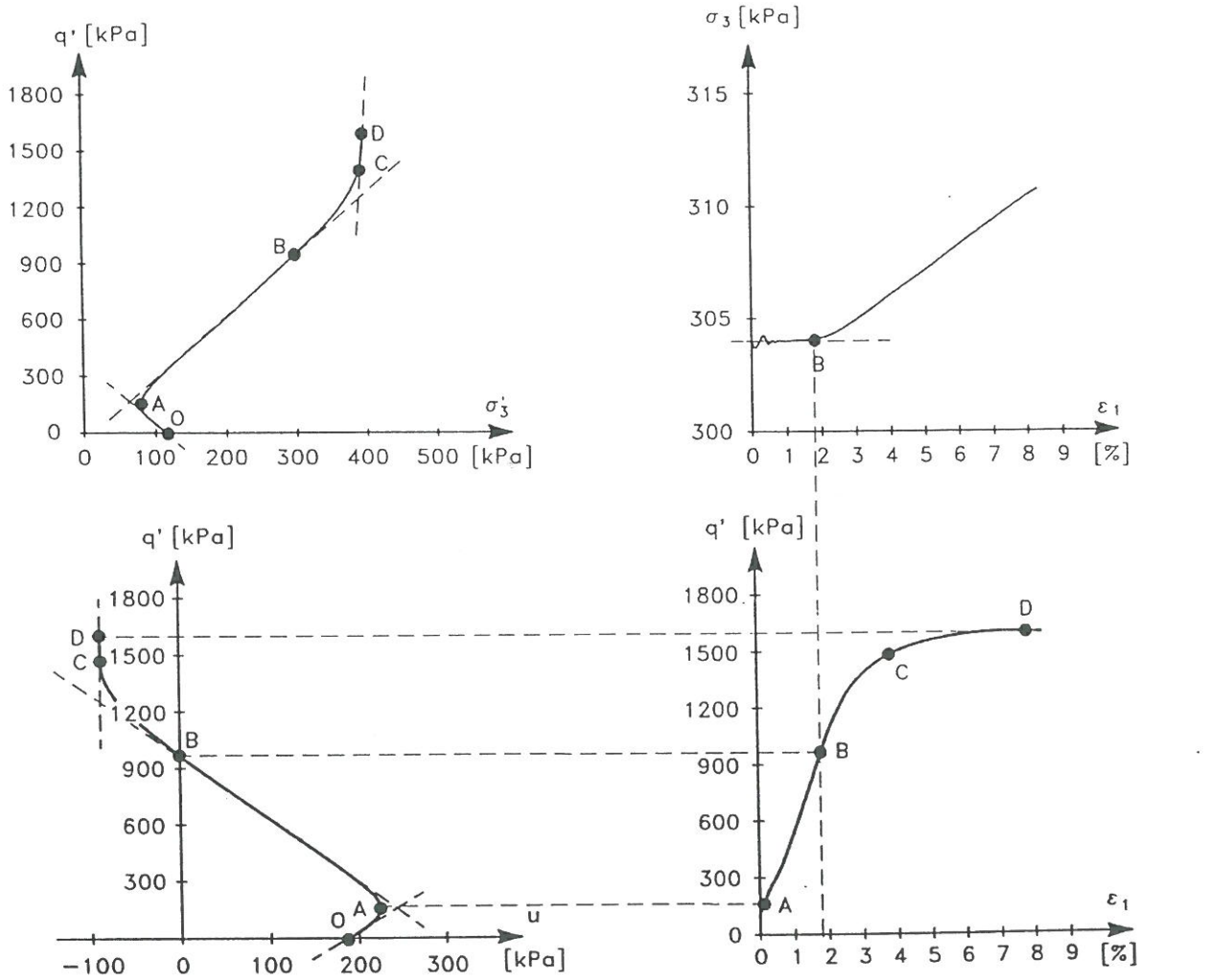

Figure 20. Results of a high deformation rate CU-triaxial test performed on Aalborg University sand No 1. The tests was performed with a constant deformation rate of 1000 % per hour. The specimen was prepared with $I_D = 0.80$.

The variation of the pore pressure during a high deformation rate CU-test is outlined in Figure 20. The figure shows that the pore pressure initially increases to prevent the sand from contraction and $\delta u > 0$. When the deviator stress approaches the characteristic stress state, point A, $\delta u \to 0$. Between point A and B the pore water manages to prevent the sand from dilating and the pore pressure generation is negative, $\delta u < 0$. Up to point B the stress-strain curve, Figure 20d, shows the same strain hardening response as outlined in Fig. 19b, and the stress path follows the common stress path defined by the drained stress states where $\Sigma \delta \varepsilon_v = 0$. When the pore pressure becomes negative the response changes character. The pore water can no longer prevent interlocking disrupture and the material starts to dilate slightly. The dilation causes a strengthening of the material and the response starts to deviate from the common stress path. At point C the pore water provides the maximum resistance and cavitation occurs at approximately -90 kPa. From this state the effective confining pressure remains constant, and further strengthening of the material depends entirely on the dilation. At point D failure occurs, while the negative pore pressure remains constant and does not vanish between C and D, as shown in Figure 20.

A static test is shown in Figure 21. At first, the test is performed as a constant volume test, $CU_{u=0}$ test. After the stress path has followed the common stress path for a while, the undrained restriction is changed to a drained conditions. It is seen that the shift from undrained to drained conditions results in dilation and the observed response is identical to that outlined in Figure 20. It is clearly shown, that the stress path during the drained part of the test in Figure 21 is identical with stress path C - D in Figure 20. It clear that drained failure conditions control failure in both tests, even though the overall conditions are undrained in the CU-test in Figure 20.

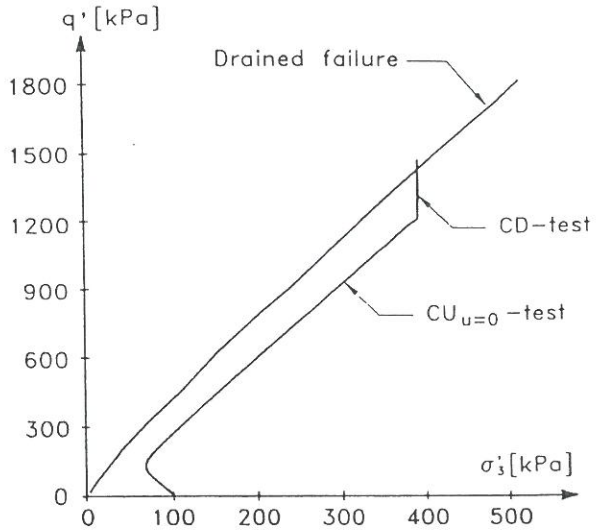

Figure 21. Static $CU_{u=0}$/CD triaxial compression test on Aalborg University sand No. 1. The test was performed with constant deformation rate of 4 % per hour and I_D = 0.80.

If the soil element is located at a water depth where the hydrostatic pressure is high enough to prevent dilation, failure occurs at the intersection point between the characteristic line and the drained failure surface, as shown in Figure 3 and 4. Thus again, the drained failure surface is seen to control failure even though the overall conditions are undrained.

7.2 Deformation rate effects

The effect of deformation rate on the sand behavior has been studied by performing triaxial tests with constant deformation rates varying from 40 to 100,000 % per hour. The result of this study is outlined in Figures 22 and 23. The ratio between the dynamic and the static strengths is 1.1 for the tests shown in Figure 22. It has been speculated before (Nash and Dixon 1961, Yamamuro and Lade 1993) that the lower undrained strengths observed in the static tests are caused by higher pore pressures generated at low strain rates where more time is available for particle crushing and rearranging. This would result in more volumetric compression, but since the tests were undrained, higher pore pressures were induced. At higher strain rates, less time was allowed for particle crushing and rearranging to occur, and this caused the specimen to be less compressive. Consequently, lower pore pressures were produced and higher deviator stresses were obtained.

The stress-strain curves shown in Figure 23 indicate considerable rate effects. These effects are important in analyzing the interaction between the

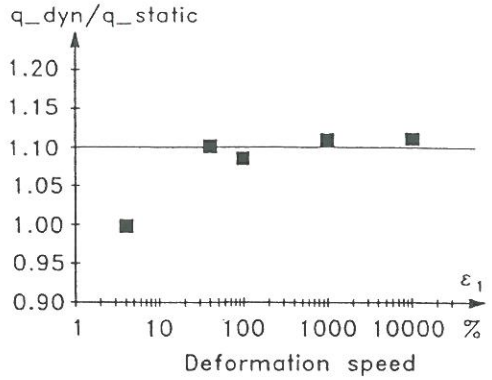

Figure 22. Relative strengths of CU triaxial tests on Aalborg University sand No. 1, I_D = 0.80. The tests were performed with constant deformation rates varying from 40 to 100,000 % per hour.

structure and the soil when calculating the dynamic amplification factors.

7.3 Effects of height-to-diameter ratio

As discussed above, a tall specimen may not be capable of producing uniform deformation conditions throughout a triaxial test. This has considerable influence on the results of undrained tests. Test results of drained and undrained triaxial tests performed on specimens with homogeneous stress and strain distributions are shown in Figure 24a. The same sand was also tested in an undrained triaxial test with the height of the specimen equal to twice the diameter, as shown in Figure 24b. Initially the

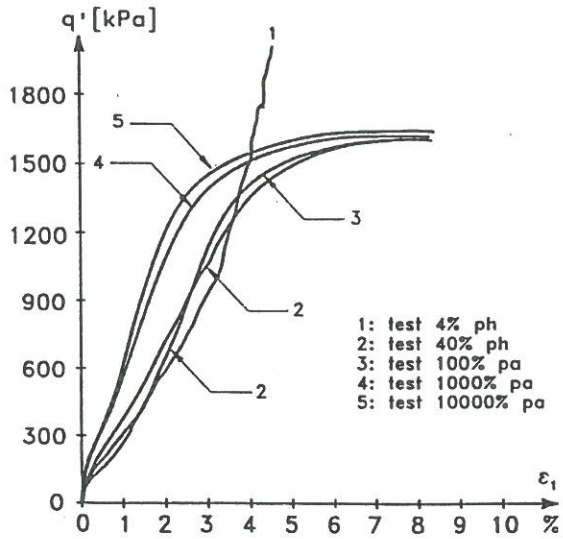

Figure 23. Stress-strain curves from triaxial tests on Aalborg University sand No. 1 performed with different deformation rates. Strength comparisons shown in Figure 22.

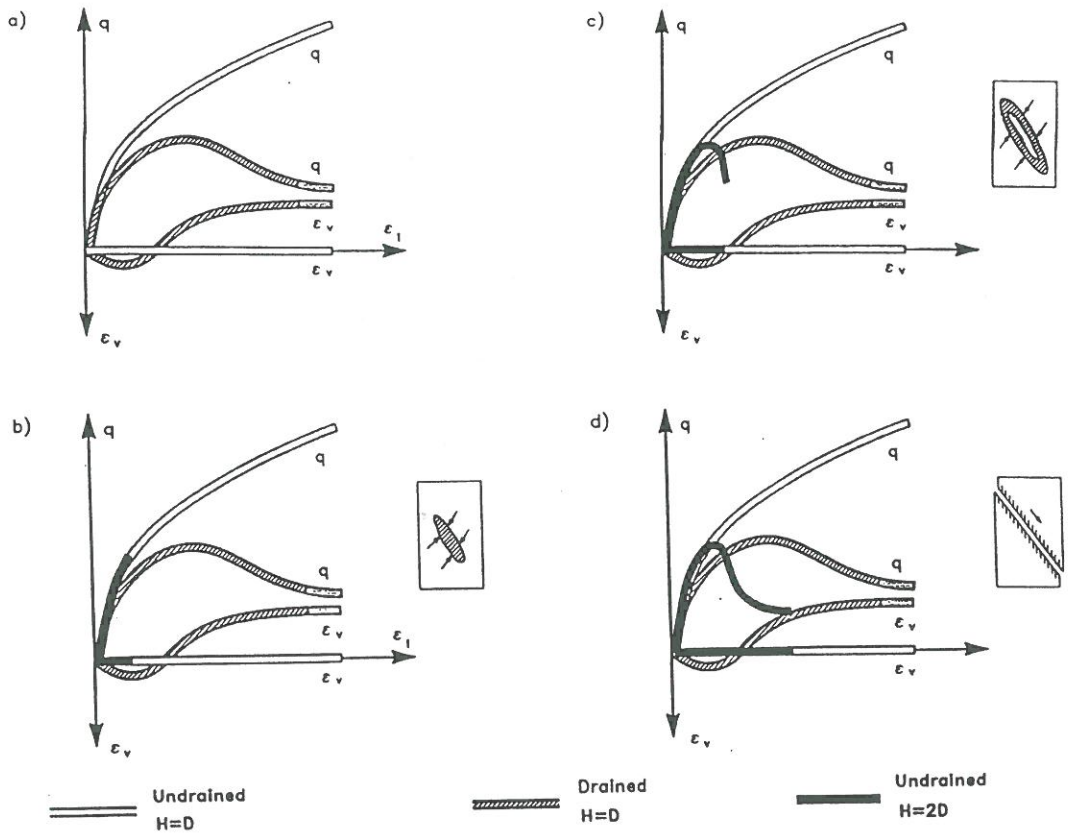

Figure 24. The consequence of an undrained test performed on a specimen with double height. (a) Drained and undrained test with homogeneous strain conditions. (b) Development of the locally weakened zone in which the shear plane subsequently is formed. (c) The drained zone dominates the stress-strain curve. (d) Two practically solid bodies sliding past each other (H = height and D = diameter of the specimen).

two stress-strain curves from the undrained tests coincide. As the deviator stress q increases, the sand will try to expand. Under homogeneous conditions this expansion is impossible since the drains are closed. The resulting pore water suction will increase and hold the grain structure together. But in the tall specimen the deformation is not homogeneous, and some local zones will dilate and others will contract, resulting in zero overall volumetric strain. Inside the specimens water will flow from the zones that contract to the zones that dilate, as shown on the insert in Figure 24b. As a consequence, the test is not truly undrained, even though the overall volume of the whole specimen is kept constant. The stress-strain curve corresponding to these opposing volume change tendencies begin to deviate from the curve obtained from the uniform strain test as the zones with nonuniform strains develop into more distinct

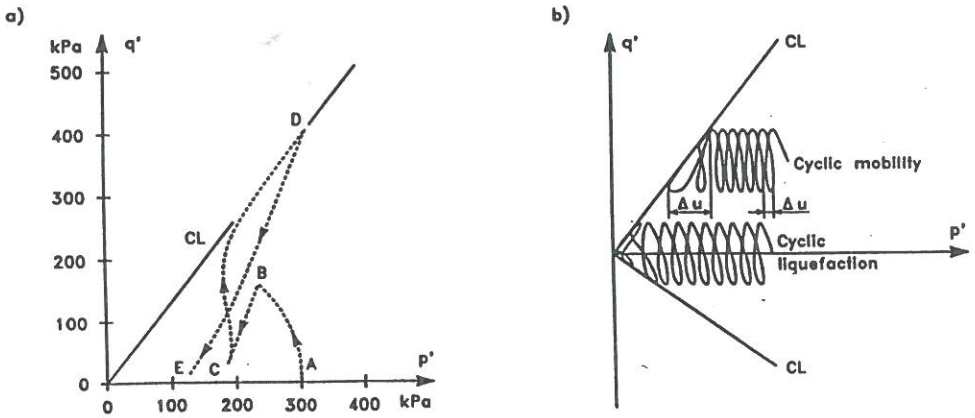

Figure 25. Results of CU-tests performed on specimen with double height submitted to a) static loading, b) cyclic loading. (Ibsen 1995).

localized zones, as illustrated on the insert in Figure 24c. Consequently, the inner drainage of some portions of the tall specimen causes the externally measured stress-strain curve to resemble the curves from the fully drained tests shown in Figure 5b. Critical state conditions develop inside the localized shear zone as the test continues. A shear band develops, and two practically solid bodies slide past each other, as indicated on the insert in Figure 24d. This limits the full development of negative pore pressure, and the shear strengths from such tests are consequently too low.

Figure 25 shows the results of CU-tests conducted on specimens with double height submitted to a) static loading and b) cyclic loading. Similar to the results in Figure 19a, the pore pressure in Figure 25a increases in the beginning, but as soon as the deviator stress approaches the characteristic line cl, the localized zone starts to develop. The inner drainage in the nonhomogeneous specimen causes reduced suction. As a consequence the effective stress path cannot be located correctly in the dilation subspace. In Figure 25a the test results show that the effective stress path therefore follows the characteristic line cl when the characteristic threshold is reached. This has led to the opinion that the undrained failure envelope describes a straight line through the stress origin.

In the case of undrained cyclic loading the stress variation can only be located in the subspace which is characterized by contraction and the stress variation will therefore always lead to pore pressure buildup. If the cyclic loading involves negative deviator stresses and the number of cycles is large enough, the effective stress variation will approach the characteristic line cl. Similar to static loading, the localization zone starts to develop and the stress variation is seen in Figure 25b to follow the characteristic line in both compression and extension. This phenomenon is described by many authors and called *Cyclic Liquefaction* (initiated by Seed and Lee 1966). If the cyclic loading involves negative deviator stresses, *Cyclic Mobility* can occur as described by Casagrande (1971). In both phenomena the shear plane is developed progressively as the cyclic stress variation continues to follow the characteristic line in each cycle. Large residual deformations are observed and the phenomenon is normally considered an expression of failure due to cyclic loading. As the effective stress variation follows the same effective stress path, both under cyclic and static loading, the "Undrained failure envelope" - which is seen to be identical to the characteristic line - is widely accepted to control the development of failure due to cyclic loading, see for instance Guzmann et al. (1988).

8 CONCLUSIONS

By studying the basic sand behavior in triaxial tests under uniform conditions, identical responses of the sand due to static and dynamic loading have been discovered. The static and dynamic responses of sand can be explained with help of the characteristic state, and the strength of sand under undrained conditions is found to be controlled by the drained failure condition for both static and dynamic loading.

The negative pore pressure remains during failure Thus, the negative pore pressure can be counted on as a reliable stabilizing factor in calculations for design of foundations subjected to variable or dynamic loads.

The ratio between the dynamic and static strengths is approximately 1.1 in the interval from 40 to 100,000 % per hour. The tests also showed that the stress-strain curves indicated great rate effects. These effects are important in analyzing the interaction between the structure and the soil when calculating the dynamic amplification factors.

In this paper, the characteristic state is redefined as the stress state where $\delta\varepsilon_v$ becomes zero for the first time in a test with $p' = const.$ Further, the phase transformation state is defined as the state where $\delta p'$ becomes zero for the first time. As a consequence, the characteristic and phase transformation lines become identical. These definitions are mutually consistent, and they may therefore be useful in controlling the plastic potential function for description of plastic volume changes of soils.

In comparison, the characteristic angle defined by Luong (1982) is not an intrinsic parameter, independent of stress path, and it not useful for development of elasto-plasticity models.

The characteristic line has been studied in view of experimental results from drained and undrained triaxial compression tests and cubical triaxial tests on different sands. Experiments have shown, that the relative density and the minor principal stress do not influence the location of the redefined characteristic line and the characteristic angle is therefore unique for a given sand.

It is also shown that nonuniform deformations, which develop at very small strains in tall specimens, may influence the measured characteristic angles and the conclusions regarding the effect of the minor principal stress. It is therefore recommended to determine the characteristic and the phase transformation states from experiments with uniform stress and strain states. These are best produced in tests on specimens with height equal to diameter and lubricated ends.

REFERENCES

Bishop, A.W. and Green, G.E. 1965. The influence of end restraint on the compression strength of a cohesionless soil. Geotechnique, 15(3), 243-266.

Casagrande, A. 1971. On Liquefaction phenomena. *Geotechnique,* September, 1971 XXI(3), 197-202.

De Groot, M.B, Andersen K.H, Burcharth H.F, Ibsen. L.B, Kortenhaus. A, Lundgren H, Magda W, Oumeraci H, Richwien W. Foundation Design of Caisson Breakwaters. *Norwegian Geotechnical Institute. Publicatio No 198. Volume 1.*

Guzmann, A. A. et al. 1988. Undrained monotonic and cyclic strength of sand. *Jurnal of the Geotechnical Engineering Division ASCE*, 114(10), 1089-1118.

Ibsen, L.B. 1994. The stable state in cyclic triaxial testing on sand. *Soil Dynamics and Earthquake Engineering 13,* 63- 72.

Ibsen, L.B 1995. Static and dynamic strength of sand. *Eleventh European Conference on Soil Mechanics and Foundation Engineering*, Copenhagen, Denmark, 29 May - 1 June.

Ibsen, L.B. and Bødker, L. 1994. Baskarp Sand No. 15. *Data Report 9301*, Soil Mechanics Laboratory, Aalborg University, Denmark.

Ibsen, L.B and Lade P.V. 1998. The Role of the Characteristic Line in Static Soil Behavior. 4th Workshop on Localisation and Bifurcaton Theory for Soils and Rocks, A. A Balkema.

Ibsen, L.B. and Jakobsen, F.R. 1996. Lund Sand No. 0, *Data Report 8401, 8402, 8801 & 8901,* Soil Mechanics Laboratory, Aalborg University, Denmark.

Ishihara, K., Tatsuoka, F. and Yasuda, S. 1975. Undrained deformation and liquefaction of sand under cyclic stresses. *Soils and Foundations,* 15(1), 29-44.

Jacobsen, M. 1967. The undrained shear strength of preconmsolidated boulder clay. *Proc. Geot. Conf.*, Oslo, I, 119-122.

Jacobsen, M. 1970. New Oedometer and Triaxial Apparatus for Firm Soil. *DGI Bulletin No. 27*, 7-20.

Jacobsen, M. 1981 Two Comments on Laboratory Tests. Proc. 10th Int. Conf. Soil Mech. Found. Engr., Stockholm, Sweden.

Jakobsen, F.R. and Simonsen, J. 1994 Horizontal resistance of dynamically loaded piles. (in Danish). *M.Sc. Thesis.* Aalborg University.

Lade, P. V. 1982. Localization effects in triaxial test on sand. *IUTAM Conference on Deformation and Failure of Granular Materials*. A.A. Balkema, Rotterdam, 461-471.

Lade, P.V. 1994. Instability and Liquefaction of granular materials. Computers and Geotechnics, 16, 123-151.

Lade, P.V. and Duncan, J.M. 1973. Cubical triaxial tests on cohesionless soil. *Journal of the Soil Mechanics and Foundations Division,* ASCE, 99(10), 793-812.

Lade P.V and Ibsen 1997. A Study of the Phase Transformation and the Characteristic Lines of Sand Behavior. *Deformation and Progressive failure in Geomechanics. IS-NAGOYA '97.* Pergamon Press, 353-358.

Lade, P.V. and Prabucki, M.-J. 1995. Softening and preshearing effects in sand. *Soils and Foundations,* 35(4), 93-104.

Lee, K.L. 1965. Triaxial compressive strength of saturated sand under seismic loading conditions, PhD thesis, University of California, Berkeley.

Lee, K.L. and Seed, H.B. 1967. Drained strength characteristics of sands. *Journal of the Soil Mechanics and Foundations Division,* ASCE, 93(6), 117-141.

Luong, M.P. 1982. Stress-strain aspects of cohesionless soils under cyclic and transient loading. *International Symposium on Soil under Cyclic and transient Loading,* A. A Balkema, Rotterdam, 315-324.

Nash, K.L. and Dixon, R.K. 1961. The measurement of pore pressure in sand under rapid triaxial tests, *Proc. Conf. on the pore pressure and suction in soils*, Butterworths, London, 21-25.

Rowe, P.W. and Barden, L. (1964). Importance of free ends in triaxial testing. *Journal of the Soil Mechanic and Foundation Division, ASCE,* 90(SM1), 1-27.

Yamamuro, J.A. and Lade, P.V. 1993. Effects of strain rate on instability of granular soils, *Geot. Testing J.,* 16(3), 304-313.